

# The Stiffness of Plasma Sprayed Zirconia Top Coats in TBCs

J.A. Thompson, T.W. Clyne, University of Cambridge, Cambridge, UK.

## Abstract

Yttria-stabilised zirconia coatings have been deposited onto nickel superalloy substrates by air plasma spraying (APS). Free standing layers were then obtained by chemical dissolution techniques. The in-plane Young's modulus values exhibited by these layers were measured using the techniques of cantilever bending and ultrasonic resonant frequency testing during flexural vibration. Young's modulus data were also obtained by nanoindentation of regions remote from microcracks. The values obtained by bending and frequency measurement were found to be considerably lower than that expected for bulk zirconia, whereas those obtained by the nanoindentation experiments were much closer to that of the bulk ceramic. Tests were also performed on samples which had been heat treated at 1100°C and 1300°C. It was found that the stiffness rose significantly after such treatments. This is attributed to sintering processes which generated extensive healing of microcracks.

## 1 Introduction

Since nickel superalloy components in advanced gas turbine engines now operate at temperatures very close to the theoretical limits imposed by the onset of liquation, current strategies for performance improvements are centred on thermal barrier coatings (TBCs). Typical current TBC systems[1, 2] are composed of a ZrO<sub>2</sub>-(6 to 8 wt.%) Y<sub>2</sub>O<sub>3</sub> ceramic top coat about 300-500 µm in thickness, deposited either by air plasma spraying (APS) or electron beam assisted physical vapour deposition (EB-PVD), over an MCrAlY (M = Ni, Co or NiCo) bond coat, about 100 µm thick, deposited by vacuum plasma spraying (VPS).

Plasma sprayed zirconia is primarily composed of the metastable tetragonal (t') phase[3]. Other features of note in the as-sprayed microstructure include the layered, plate-like splats, which in turn usually consist of several individual columnar grains of zirconia. APS zirconia usually exhibits a high level of porosity (typically ~12-15%). Two types of pore are commonly present - interlamellar porosity caused by poor bonding between splats and a network of through-thickness microcracks, which forms during the rapid cooling of individual splats[4, 5].

These features of the microstructure contribute to the low thermal conductivity of APS zirconia compared with the bulk ceramic[6, 7] and are also thought to raise its strain tolerance. However, the precise way in which this high strain tolerance arises is still rather unclear. Recent work on the stiffness of plasma sprayed zirconia[5, 8, 9] has indicated that its value may be relatively low, but also that the value obtained can depend significantly on the measuring technique employed. In the present paper, the stiffness of as-sprayed zirconia is measured using three different techniques and the effect of post-deposition heat treatment on the value obtained is also explored

## 2 Experimental Procedures

### 2.1 Specimen Preparation

Samples were prepared by air plasma spraying of Zirspra 9507 8wt% yttria ZrO<sub>2</sub> powder. The spray parameters used are given in **table 1**. Nickel superalloy (Nimonic 80A) substrates were grit blasted with alumina prior to coating deposition. Samples for cantilever beam testing were sprayed to a thickness of approximately 500 µm, corresponding to 4 passes of the plasma spray gun, while samples for ultrasonic testing and nanoindentation were sprayed to a thickness of 2 mm (15 gun passes).

Spray Type	APS
Stand-off Distance (mm)	100
Arc Current (A)	600
Arc Voltage (V)	70
Ar flow rate (SLPM)	60
H <sub>2</sub> flow rate (SLPM)	10
Gun Speed (mm s <sup>-1</sup> )	50
Carrier gas flow rate (SLPM)	6
Disc Speed (%max)	20
Stirrer speed (%max)	80
Nozzle Diameter (mm)	8

**Table 1:** Parameters for plasma spraying of zirconia.

APS zirconia coatings were detached by etching in concentrated HCl, which led to attack of the interface between substrate and coating and

caused debonding of the ceramic layer. Heat treatment of these layers was performed at 1100°C and 1300°C, for periods of up to about 100 hours.

Samples for cantilever bend testing and ultrasonic resonant frequency measurement were cut to the required dimensions using a diamond wheel on a slow speed Accutom saw. Sample dimensions were 50 x 20 x 0.5 mm for cantilever bending and 50 x 10 x 2 mm for resonance testing. Samples for nanoindentation were prepared by hot mounting and polishing the top surface of the coating to a 0.25 µm finish. Specimens were then removed from the mounting material and secured onto nanoindentation stubs.

## 2.2 Stiffness Measurement

### 2.2.1 Cantilever Bend

One end of the specimen was clamped in a cushioned vice. Weights of increasing magnitude were then applied near to the free end of the specimen. A non-contacting laser scanning extensometer (Lasermike) was used to monitor the displacement of the beam for each applied load. The Young's modulus,  $E$ , of the material in bending was then calculated using Equation 1.

$$E = \frac{P}{yI} \frac{Lx^2}{2} - \frac{x^3}{3} \quad (1)$$

where  $L$  is the distance from the clamped end to the loading point,  $I$  is the second moment of area of the sample,  $P$  is the applied load and  $y$  is the deflection measured at a distance  $x$  from the clamped end.

### 2.2.2 Ultrasonic Resonance.

Ultrasonic testing was performed on a Grindo-Sonic MK5 frequency analyser. The specimen for testing is supported at two points, about 22% of the specimen length from each end. A light mechanical impulse is applied, to excite the fundamental flexural vibration in the specimen, the nodes of which are located at the support points. The period of the resonant vibration is displayed a few seconds later. A computer program (EMOD), developed by J.W. Lemmens Elektronika N.V. was used to determine the Young's modulus,  $E$ , from the resonant frequency and specimen geometry, according to equation 2:

$$E = 0.94642 \frac{\rho L f^2 \Gamma}{h^2} \quad (2)$$

where  $\rho$  is the density,  $L$  is the specimen length,  $f$  is the resonant frequency and  $\Gamma$  is a correction factor dependent on the sample width, length and Poisson ratio.

### 2.2.3 Nanoindentation.

Nanoindentation was carried out using a Micro Materials Nano Test 600 indenter. A microscope allows the user to pinpoint the position at which an

indent is to be made. Indents were performed in regions remote from visible cracks. A series of indentation experiments was performed on two samples. One of these was in the as-sprayed condition, while the other had been subjected to a heat treatment at 1300°C for 88 hours. In each case the indentation conditions were identical, with a maximum load of 100 mN and a loading rate of 4.1 mN s<sup>-1</sup>.

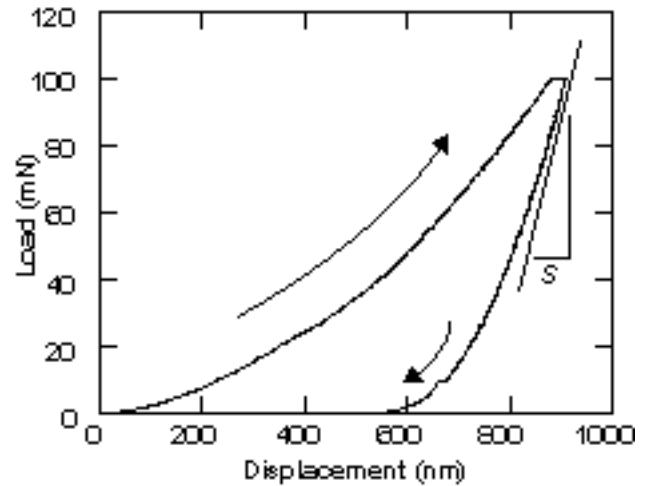


**Fig. 1:** Plot of load against depth during nanoindentation.

An example of a load / displacement plot obtained during indentation of as-sprayed zirconia is shown in **Fig. 1**. The Young's modulus of the sample material ( $E_s$ ) is obtained from the gradient of such a plot at the onset of unloading,  $S$ , according to Equations 3 & 4.

$$S = \frac{dP}{dh} = \sqrt{\frac{4A}{\pi}} E_r \quad (3)$$

$$\frac{1}{E_r} = \frac{(1 - \nu_s^2)}{E_s} + \frac{(1 - \nu_i^2)}{E_i} \quad (4)$$

where  $P$  is the applied load,  $h$  is the indentation depth,  $A$  is the contact area,  $\nu$  is the Poisson ratio and the subscripts  $r$ ,  $s$ , and  $i$  correspond to the reduced modulus of the system, the sample material and the indenter material (diamond). The Oliver and Pharr[10] method was used to determine the value of the gradient,  $S$ , allowing for the curvature of the unloading plot

## 3 Measured Young's Modulus Values

### 3.1 Assessment of Techniques

#### 3.1.1 Cantilever Bend

Some hysteresis was observed in the loading / unloading plots - see **Figure 2**. This effect was most significant for samples in the as-sprayed condition or after limited heat treatments. It can be attributed to the opening of cracks during loading, which do not then close fully on removal of the

applied load. Samples loaded and unloaded several times showed diminishing hysteresis.

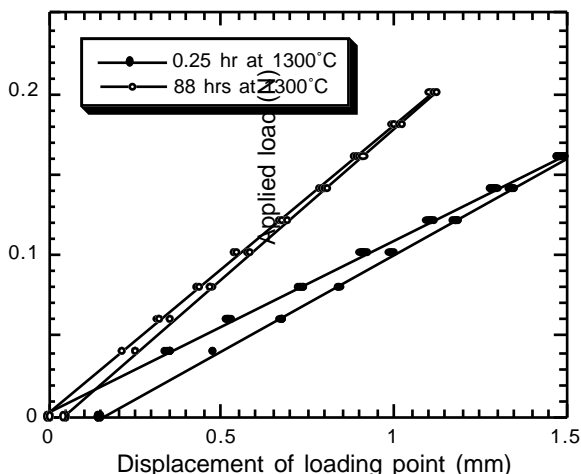


**Fig 2:** Force-displacement plots for cantilever beam bending of two specimens subjected to different heat treatments.

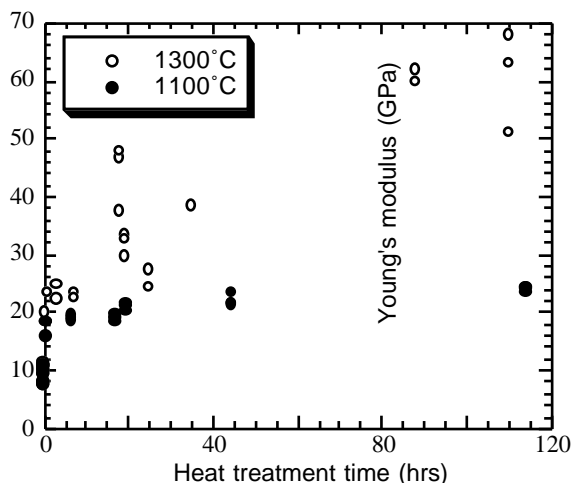


**Fig 3:** Young's modulus data obtained by cantilever bending, as a function of heat treatment time.

Cantilever beam bending results are shown in **Figure 3**. Several trends are discernible:

- i The Young's modulus of as-sprayed material is about 10 GPa. This is in good general agreement with most data in the literature[5, 8, 9, 11]. The value is considerably lower than that of bulk zirconia (180-200 GPa). This is attributed to the presence of defects, particularly the high density of through-thickness microcracks. These can be clearly seen in the SEM image of Figure 4, showing the free surface of an as-sprayed coating.
- ii The effect of heat treatment on the stiffness of APS zirconia is significant. This is particularly true for the higher heat treatment temperature of 1300°C, which generated a six-fold increase in stiffness after 100 hours. This rise in stiffness

can be divided into two regimes. In the early stages of heat treatment ( $t < 1$  hour), there is a sharp increase in modulus, which approximately doubles in value. It is proposed that this is due to the "healing" of small defects in the sprayed microstructure. Such a step-like change in material properties after short sintering times has also been observed by Eaton and Novak[12]. While pronounced sintering of ceramics is not in general expected at temperatures below about 1400°C, Wesling *et al*[8] observed detectable effects in plasma sprayed zirconia at temperatures as low as 800°C.

**Fig. 4:** SEM micrograph of the free surface of an as-sprayed coating, showing extensive microcracking.

**Fig. 5:** SEM micrograph of the free surface of a coating after heating at 1400°C for 6 hours, showing sealing of microcracks.

- iii During longer heat treatments, the stiffness of the top coat continues to rise progressively. This is associated with relatively slow repair of larger defects in the microstructure. As expected, this effect is more pronounced at the higher sintering temperature. A micrograph showing a sintered microstructure, incorporating

healed microcracks, is shown in **Figure 5**. Grain growth across splat boundaries is also known to occur[12] and there will also be a contribution to material stiffening as a result of this effect. Ibegazene *et al*[9] noted similar trends in the stiffening of APS zirconia over long periods.

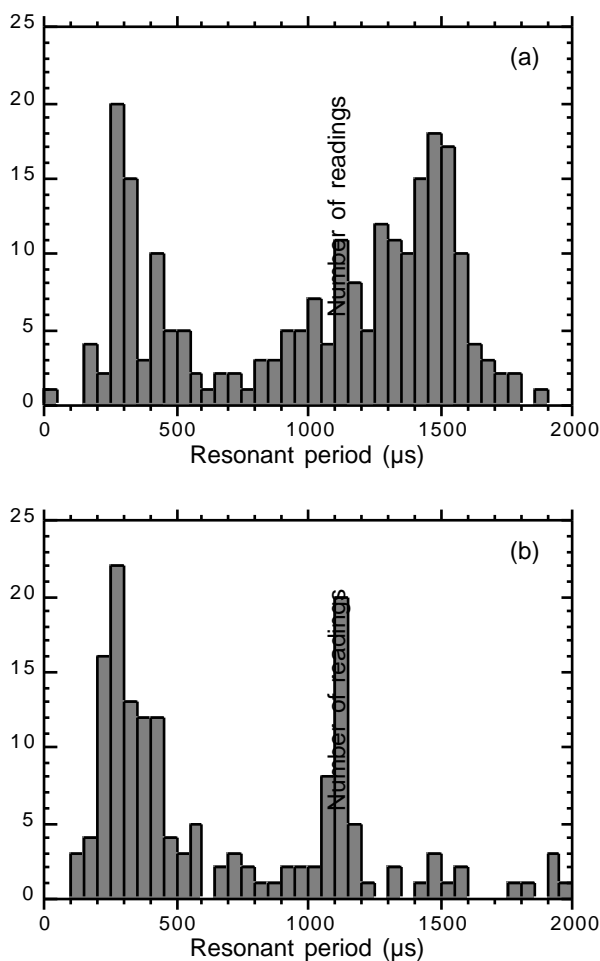


**Fig 6:** Distribution of measured resonant period data obtained from (a) an as-sprayed specimen and (b) a specimen heat treated for 6 hours at 1300°C.

### 3.1.2 Ultrasonic Resonance

Excitation of the fundamental vibration in a fully dense, uncracked specimen is a simple process, and a consistent value for the measured period of oscillation is expected. However, the nature of the microstructure of APS zirconia introduces the possibility of more complex vibrational effects being observed. In an attempt to explore such effects, a large number of readings (~200) were taken from a particular as-sprayed specimen. The values obtained are plotted on the histogram shown in **Figure 6(a)**.

Two distinct peaks are observed in the distribution of data, centred at 290  $\mu\text{s}$  (mode I vibration) and 1480  $\mu\text{s}$  (mode II vibration). These vibrational periods correspond to Young's modulus values of about 200 GPa and 10 GPa respectively. (The relationship between measured period and inferred

Young's modulus, for the specimen dimensions concerned, is shown in **Figure 7**.) The mode II vibration apparently occurs when the sample as a whole, inclusive of all the defects present, is excited into its fundamental vibration. The modulus value corresponding to this resonant mode is observed to be close to that obtained by cantilever bending, which is consistent with this explanation.

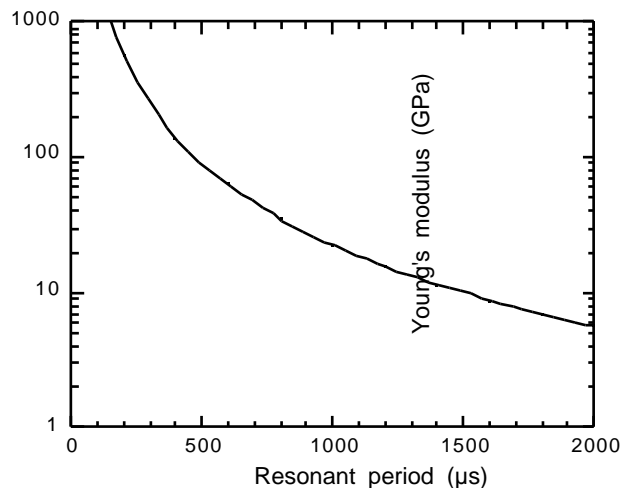


**Fig 7:** Dependence of the deduced Young's modulus value on the measured resonant period, for specimens having the dimensions of those in the current work.

Mode I vibration appears to occur when one of the small, uncracked regions of ceramic is excited into its resonant vibration. This in turn may set neighbouring regions into vibration, so that the whole sample may effectively vibrate at the frequency associated with uncracked material. In this way, the mode I peak corresponds with a modulus of about 200 GPa, close to that of monolithic zirconia. In practice, a wide range of frequencies might be expected to arise, with various complex harmonics etc being generated, and this probably accounts for the high level of noise in the data.

**Figure 6(b)** shows a plot of the distribution in measured resonant period for a sample tested after 6 hours at 1300°C. The mode II peak has moved to a shorter period, corresponding to a Young's modulus of 20 GPa. However, there is no change in the position of the mode I peak, which still indicates a Young's modulus value of 200 GPa. These observations are clearly consistent with the above explanation and with the cantilever beam data for similar specimens.

A comparison is shown in **Figure 8** between results from the cantilever bending technique and those obtained using the resonance (mode II vibration) method. The samples in this comparison had been heat treated for various periods at 1300°C. There is good agreement between the values obtained from the two techniques, particularly for relatively short sintering times (lower stiffness values). Both methods detected the step-like change in stiffness

after short heat treatments, associated with the healing of small defects, followed by a progressive rise for longer times. For the stiffest specimen in this series, the ultrasonic modulus fell below that obtained by bending. This is probably due to the greater error in stiffness associated with uncertainties in resonant period when the material is stiffer, which is a consequence of the form of the plot shown in Figure 7.

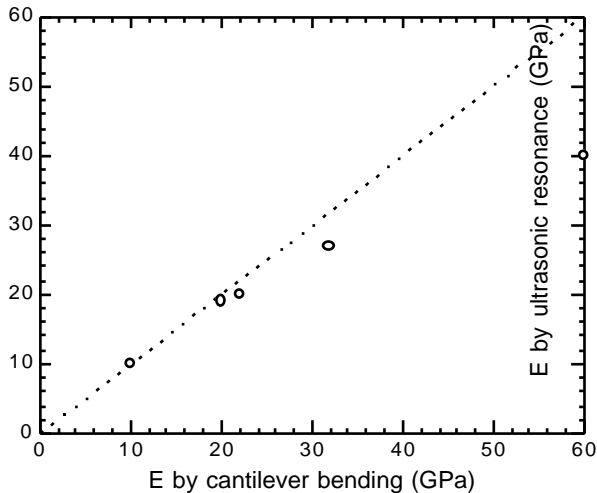


**Fig. 8:** Comparison between Young's modulus data for a series of specimens heat treated at 1300°C, obtained by ultrasonic resonance and cantilever bending techniques.

### 3.1.3 Nanoindentation

Young's modulus data were obtained by indentation in regions remote from visible cracks. The average value was found to be 135 GPa in the as-sprayed condition. This value is consistent with the observed microstructure, consisting of a network of cracks and pores separating regions of uncracked material. The area of the indentation was small (sub-micron), so that a value for the modulus is expected which approaches that of the monolithic ceramic. The fact that the measured value is somewhat below the nominal value for dense material can be explained in terms of the presence of subsurface flaws and porosity.

The measured value for a sample heat treated for 93 hours at 1300°C was found to be 205 GPa, which is close to the nominal value for bulk zirconia, within the error associated with the nanoindentation technique[10]. This suggests that effects such as healing of microcracks and reduction in porosity have removed the effect of flaws on the measurement.

## 4 Summary

The following points should be noted about the work described in this paper.

- i The Young's moduli of APS  $ZrO_2 - 8wt\%Y_2O_3$  coatings have been measured using three

techniques; cantilever beam bending, ultrasonic resonance and nanoindentation.

- ii The macroscopic in-plane modulus in the as-sprayed condition is about 10 GPa, which is much lower than that of monolithic zirconia (~200 GPa). This is attributed to the presence of defects in the sprayed microstructure, such as interlamellar porosity and, particularly, through-thickness microcracks.
- iii Heat treatment can raise the stiffness considerably. For example, even an hour or so at 1300°C leads to a doubling of the stiffness, while a six-fold increase results after 100 hours. Some stiffening was also observed at the lower temperature of 1100°C, but the effects were less pronounced. Microstructural examination indicated that the most significant change during heat treatment was the healing of microcracks.
- iv The cantilever bend technique, employed with a high precision scanning laser method of displacement measurement, was found to be the most reliable procedure. Ultrasonic resonance measurement also gave consistent stiffness data, although careful interpretation was needed to avoid confusion from the excitation of various extraneous vibration modes. The nanoindentation procedure can be used to obtain the local stiffness between defects, which is considerably higher than the macroscopic in-plane stiffness of these coatings.
- v The macroscopic Young's modulus values obtained are averages from compressive and tensile loading. From the nature of the defects present, it is expected that the stiffness will be appreciably higher in compression, particularly at relatively high strains (when microcracks will start to close up). Quantification of this effect is the subject of ongoing work.

## 5 Acknowledgements

Thanks are due to EPSRC and Rolls-Royce plc for supporting the project within which this work has been carried out and also to Miss A.C. Fox for assistance with some of the experimental work and for various helpful discussions.

## 6 References

1. Joshi, S. and Srivastava, M., *On the Thermal Cycling Life of Plasma-Sprayed Ytria-Stabilised Zirconia Coatings*. Surf. Coat. Technol, **56**, (1993), p.215-224.
2. Bennett, A., Toriz, F. and Thakker, A., *A Philosophy for Thermal Barrier Coating Design and its Corroboration by 10000h Service Experience on RB211 Nozzle Guide Vanes*. Surf & Coat Tech, **32**, (1987), p.359-375.

3. Lelait, L., Alperine, S., Diot, C. and Mevrel, M., *Thermal Barrier Coatings; Microstructural Investigation after Annealing*. Mat. Sci. Eng., **A121**, (1989), p.475-482.
4. Harmsworth, P.D. and Stevens, R., *Phase Composition and Properties of Plasma-Sprayed Zirconia Thermal Barrier Coatings*. J. Mater. Sci., **27**, (1992), p.611-615.
5. Bengtsson, P., Johannesson, T. and Wigren, J., *The Microstructure and Residual Stresses of Thermally Sprayed Ceramic Coatings*, in "ITSC 98". C.C.Berndt (ed.), ASM, (1998), p.237-242.
6. Taylor, T.A., Appleby, D.L., Weatherill, A.E. and Griffiths, J., *Plasma Sprayed Yttria-Stabilised Zirconia Coatings: Structure-Property Relationships*. Surf. Coat. Technol., **43/44**, (1990), p.470-480.
7. Taylor, T., *Thermal Properties and Microstructure of Two Thermal Barrier Coatings*. Surf Coat Technol, **54/55**, (1992), p.53-57.
8. Wesling, K.F. and Socie, D.F., *Fatigue of Thick Thermal Barrier Coatings*. J. Am. Ceram. Soc., **77**, (1994), p.1863-68.
9. Ibegazene, H., Alperine, S. and Diot, C., *Yttria-Stabilized Hafnia-Zirconia Thermal Barrier Coatings: The Influence of Hafnia Additions on TBC Structure and High-Temperature Behaviour*. J. Mater. Sci., **30**, (1995), p.938-51.
10. Oliver, W.C. and Pharr, G.M., *An Improved Technique for Determining Hardness and Elastic Modulus Using Load and Displacement Sensing Indentation Experiments*. J. Mater. Res., **7**, (1992), p.1564-1583.
11. Tsui, Y.C., *Adhesion of Plasma Sprayed Coatings*, PhD thesis, University of Cambridge, Cambridge, UK, (1996),
12. Eaton, H.E. and Novak, R.C., *Sintering Studies of Plasma Sprayed Zirconia*. Surf. Coat. Technol., **32**, (1987), p.227-236.